Brain-Mimicking Phantom for Photoablation and Visualization

Ravi Prakash[a *], Kent K. Yamamoto[a], Siobhan R. Oca, Ph.D.[a], Weston Ross, Ph.D.[b], Patrick J. Codd, M.D.[a,b]

***Abstract*— While the use of tissue-mimicking (TM) phantoms has been ubiquitous in surgical robotics, the translation of technology from laboratory experiments to equivalent intraoperative tissue conditions has been a challenge. The increasing use of lasers for surgical tumor resection has introduced the need to develop a modular, low-cost, functionally relevant TM phantom to model the complex laser-tissue interaction. In this paper, a TM phantom with mechanically and thermally similar properties as human brain tissue suited for photoablation studies and subsequent visualization is developed. The proposed study demonstrates the tuned phantom response to laser ablation for fixed laser power, time, and angle. Additionally, the ablated crater profile is visualized using optical coherence tomography (OCT), enabling high-resolution surface profile generation.**

Keywords - Tissue Mimicking Phantom, Brain Tissue, Photoablation, Laser Surgery, Surgical Robotics

I. Introduction

The development of minimally invasive surgical technologies requires simultaneous improvement in tissue-mimicking (TM) phantoms for realistic testing conditions. Research in developing phantoms has been motivated by the desire to identify the tissue properties responsible for generating certain tissue responses to surgical instruments or visualization techniques. Tissue-mimicking phantoms developed over the years can be broadly categorized as phantoms i) to mimic tissue material property [1]–[3], ii) for surgical instrument testing [4]–[8], iii) for digital reconstruction and visualization [9], [10].

In this paper, we introduce a functionally tunable brain-mimicking (BM) phantom for photoablation studies and subsequent visualization using optical coherence tomography(OCT) for neurosurgical application. This work addresses the following research objectives

1) Design and tuning of the elastic property of BM phantom
2) Design and tuning of thermal property of BM phantom
3) Optical compatibility of BM phantom for OCT visualization
4) Response of tuned BM phantom to photoablation

The ideal BM phantom for neurosurgical application comprises similar mechanical, thermal, and optical properties to that of brain tissues and tumors. For the application of brain tissue photoablation, the physics of laser-tissue interaction and OCT attenuation pose design constraints during development. Although laser fluence and irradiance time mainly dictate tissue resection properties [11], the elastic modulus and thermal conductivity of the brain play an important role in the resultant mechanical and thermal response during photoablation [12]–[14]. Thus, the elastic modulus and thermal conductivity of the BM phantom are tuned with the addition of a scattering agent for enabling OCT visualization.

A. Relevant Brain Tissue Properties

With various neuroanatomical components, brain tissue is inherently heterogeneous in nature. Each tissue type has a different elastic modulus. For sake of predominance, and a common anatomical location for the occurrence of both primary and metastatic tumors, the extensive cortical surface of the brain (gray matter) was chosen as an ideal type of brain tissue to mimic as the best representative. The average Young's modulus (E) for gray matter range from 1.389 $\pm$ 0.289 kPa with white matter ranging from 1.895 $\pm$ 0.592 kPa, testing with a flat-punch indenter [15]. The elastic modulus of various brain tumors is also quantified within the range of 0.17 to 16.06 kPa using a custom-built multimeter-scale indenter to observe the strain response due to an applied load [16].

Thermal properties of brain tissues have previously been reported in literature [17] for modeling and other biomedical applications. Thermal conductivity (κ) of calf brain was reported to be 0.524 W(mK)$^{-1}$ at 22 °C and 0.553 W(mK)$^{-1}$ at 33 °C [11]. The thermal conductivity of brain tissue in addition to subsequent laser-tissue response is dependent on the water content of the tissue. Brain tissue consists of approximately 76% water with a κ of 0.51 W(mK)$^{-1}$, and grey matter κ is measured between 0.53 to 0.56 W(mK)$^{-1}$ with a water composition of 83% [18]. With tissues having a high percentage of water content, the laser-water interaction influences the properties at the time of ablation when the high-energy laser beam is heating the tissue to vaporization temperature. κ for *ex vivo* calf brains have been measured to increase to 4 times the value at $97°C$ compared with κ at $22°C$ [19].

B. Tissue Mimicking Phantoms for Mechanical and Thermal Applications

TM phantoms of various mediums have been developed to test various visualization techniques and surgical instruments. They are used for testing medical imaging applications such as ultrasound [3] [20], CT scans [8], fluorescence [7] and OCT [21]. Silicone-based phantoms are developed

[a]Department of Mechanical Engineering and Materials Science, Duke University.
[b]Department of Neurosurgery, Duke University School of Medicine
* Corresponding author: ravi.prakash@duke.edu

to mimic breast tissue and tumors for testing autonomous ultrasound scanning [3], but the modulus of the silicone is too high to emulate soft tissue such as brain. Agar-gelatin phantoms with tunable electrical impedance are used for CT-visible thermal ablation [8], but the optical properties for CT visualization of the developed phantom are not discussed. Hydrogel-based phantoms [1] [2] have been demonstrated to tune the mechanical properties of brain tissue but require a minimum of two days to cast and cure the phantom for use. A combination of gellan gum and propylene glycol (PPG) has been shown to yield results for tuning both thermal and mechanical properties of TM phantoms [22]. The proposed phantom in this paper is based on the composition investigated by Chen et al. [22], but it will be mechanically and thermally tuned to the properties of brain gray matter. In addition, the proposed phantom will consist of a scattering agent for OCT visualization and a water content of over 70% due to laser-water dynamics being an integral part of laser-tissue interactions [13], [19]. Finally, the phantoms that undergo photoablation are not reusable, which promotes the need to rapidly prototype BM phantoms with minimal and cost-effective ingredients and mechanically and thermally tuned properties.

II. METHODS

A. Brain Mimicking (BM) Phantom Preparation

Preparation of the phantom involves a base matrix, a solution to tune thermal conductivity, and a scattering agent for OCT visualization. For experiments involving photoablation, the phantom needs to have high water content in order to simulate laser fluence absorption and vaporization in real tissue. Based on the suggested composition from [22], we choose high-acyl gellan gum (VWR, P.A., United States) as the base matrix for BM phantoms as it provides soft and elastic textures similar to that of brain tissue. In comparison, the low-acyl gellan gum form is suited for the firm and brittle texture generation [23]. Utilizing gellan gum also provides the ability to vary the concentration and tune the elastic modulus of the tissue developed.

Deionized water is used to hydrate the mixture. The water and mass of gellan gum required to create the desired composition are added to a beaker and covered with aluminum foil to prevent water vapor from evaporating. The mixture is heated at 120 °C on a heat plate with a magnetic stirrer for 40 minutes. The result is a homogeneous mixture which is then cured for at least 3 hours in 3D-printed molds for consistent and repeatable molding, shown in Fig. 1(a). BM phantoms of 1.0% to 2.0% gellan gum concentration are created for testing in increments of 0.1% concentration. Compositions ranging from 1.0% to 1.3% yields a material that is too soft to use in the experiments, so it is left out of the analysis.

Thermal conductivity of the phantoms is controlled by adding Propylene glycol (PPG) (0.17 $W(mK)^{-1}$) (VWR, P.A., United States), as it has a lower thermal conductivity than water (0.60 $W(mK)^{-1}$. The mass or volume fraction can also be tuned to bring down the required thermal conductivity as needed [24]. Three different compositions of gellan gum phantom (1.45%, 1.5%, and 1.7%) are used to create 10%, 20%, 30%, and 40% PPG (by volume) phantoms to test how the concentration of PPG affects gellan gum phantoms with varying elastic modulus.

Optical properties such as scattering coefficients in TM phantoms have been modified by using titanium oxide spheres but due to safety concerns with ablation of titanium oxide spheres, /textcolorred20% Intralipid emulsion (Baxter Healthcare, I.L., United States) is explored as a surrogate [7]. 0.25, 0.5, 0.75, and 1.0 mL of Intralipid emulsion are mixed in 1.45% gellan gum phantoms to determine the minimum volume of Intralipid required to properly visualize the phantom under the OCT laser.

B. Characterization of Mechanical Properties

The elastic modulus of the BM phantom samples is characterized by calculating Young's modulus (E) of the samples by indentation testing. The tests are conducted using a material testing machine with a 100N load cell (Lloyd Instruments, Bognor Regis, England) as shown in Fig. 1(b). The flat face of the load cell with an outer diameter of 13.9 mm is used as the indentation tip and linearly displaced at a rate of 0.05 mm/s until displacement reached 6 mm. Once the stress-strain curves of each sample are plotted as in Fig 2(a), a linear regression model is obtained using the first 5% of strain to determine soft materials' true Young's modulus [25], [26]. The slope of the linear stress-strain model determines E (Eq. 1) [27]:

$$E = \frac{\sigma(t)}{\delta(t)} = \frac{F(t)/A}{\Delta L(t)/L_0} \tag{1}$$

where *F(t)* is the force measurements from the load cell, *A* is the cross-sectional area of the indenting face, Δ *L(t)* is the displacement of the indenting head, and L_0 is the original height of the sample.

C. Characterization of Thermal Properties

Thermal conductivity, the constant of proportionality (κ) in Fourier's law of heat conduction in Eq. 2, is characterized using the longitudinal heat flow method [28]:

$$\frac{dQ}{dt} = -\kappa A \frac{dT}{dx} \tag{2}$$

where κ refers to thermal conductivity, the left side of the equation representing heat transfer per unit time, and with *dT* and *dx* representing the temperature and distance between thermocouples along *x*. The experimental setup is presented in Fig. 1(b). A heating pad (Protherm, M.N., United States) of heat flux per unit time (5 W/in^2) is used at 30% power as a constant heat flux source. A thin foil of aluminum is placed as a layer to cover both sides of the phantom. The thickness of the samples ranges from 3.0 mm to 5.5 mm, with the aluminum foil thickness measured at 0.04 mm. The four sides exposed to air are covered with insulating material such as cotton to prevent heat from escaping. Two J-type thermocouples (Fluke Electronics, W.A., United States), one at the base near the heat source and the other at

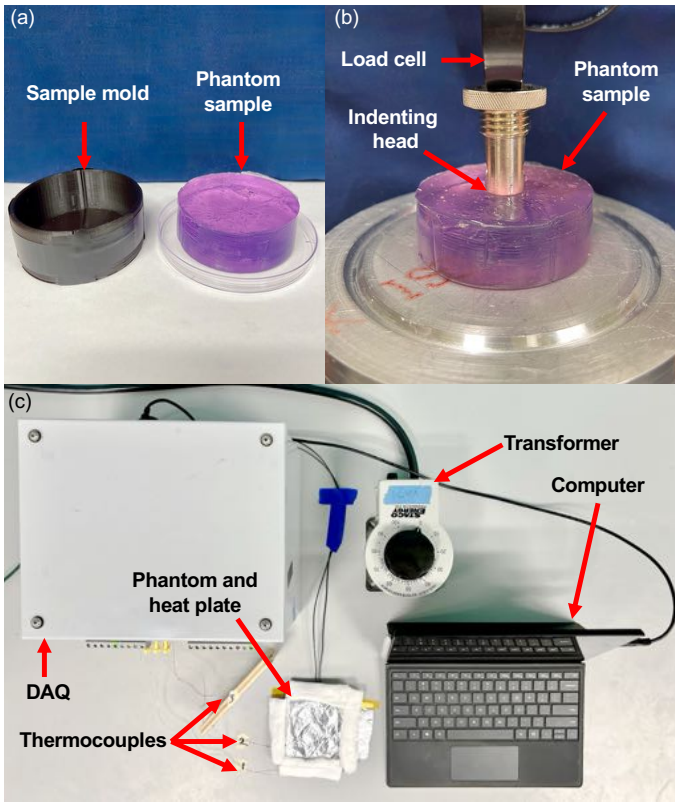

Fig. 1. (a) Cured gellan gum phantom in 3D-printed two-part mold. (b) Indentation testing setup for obtaining stress v.s. strain curves. (c) Thermal conductivity testing setup for BM phantoms.

the top surface of the phantom, are used to measure the temperature of the top and bottom sides of the phantom, similar to the method adopted in [28]. A third thermocouple is also used to record a baseline temperature value of the testing environment. A data acquisition system (National Instruments Corp, T.X., United States) is used to interface with the computer and thermocouples. Once the steady state is reached (approximately 90 minutes), the temperature difference between the two sides of the phantom is constant and the known values can be used to determine the constant of proportionality, k.

D. Photoablation and Visualization Study

The robotic laser scalpel used in this study has been developed previously for automated surface ablation studies for neurological procedures [29] [30]. In this work, a 10 W CO2 laser (Synrad Inc., W.A., United States) cuts the sample, and an inline solid-state visible red guide laser is used for guidance during sample positioning. Both lasers follow the same optic path. The lasers are outfitted with 2 galvanometers to control the point source angle with respect to the surface normal of the BM phantom. By varying the voltage supplied to the galvanometer, the incident angle can be adjusted.

For a high-resolution visualization of the photoablation crater, 1310 nm Spectral Domain - Optical Coherence Tomography (SD-OCT) (Lumedica, N.C., United States) is used. The SD-OCT system is calibrated to convert the scan to the image as mm depth and width per pixel. For calculating the depth and width of the ablated cut, a B-scan is obtained and the center of the crater observed in the B-scans is used to measure the depth and width of the cut. The samples with Intralipid emulsions are scanned to observe the visibility of gellan gum under the OCT.

TABLE I

GELLAN GUM COMPOSITION AND CORRESPONDING YOUNG'S MODULUS

Gellan Gum (% Mass)	E (kPa)
1.4	1.5075 $\pm$0.3127
1.45	2.3980 $\pm$0.3065
1.5	4.7119 $\pm$0.8235
1.6	6.3523 $\pm$0.9785
1.7	7.4092 $\pm$1.1573
1.8	13.5773 $\pm$1.2327
1.9	18.4069 $\pm$1.9105
2.0	24.2901 $\pm$2.2788

III. EXPERIMENTS AND RESULTS

A. Characterization of Mechanical Properties

Each gellan gum sample (total of 8) is indented five times and the average Young's modulus (E) from the first 5% of strain is extracted, as the viscoelastic properties of gellan gum and soft tissues react to mechanical stimulus in a nonlinear behavior [31]. Thus, the quasi-static assumption of low-frequency excitation within the first 5% of strain is utilized to observe the linear behavior of the phantom. The resultant stress-strain curves and the linear regression model implemented to obtain Young's modulus are depicted in Fig. 2(a). The stress-strain curves illustrate the increase in slope as the gellan gum concentration increases as well. After extracting E from the 40 stress-strain curves recorded, the average and standard deviations of E for each gellan gum composition are calculated, recorded in Table I, and illustrated in Fig.2(b). A linear regression model is fit to the average gellan gum Young Modulus values, and an R^2 value of 0.9486 is calculated.

After observing the data recorded and values calculated, a gellan gum phantom between 1.4% and 1.45% concentration results in Young's modulus between approximately 1.507 to 2.398 kPa. These values are within the range that Budday et al. [15] reported (1.895 $\pm$ 0.592 kPa), thus successfully tuning the gellan gum phantoms to mimic Young's modulus of brain tissue.

B. Characterization of Thermal Property

Using the 1.45% gellan gum concentration determined after tuning for the proper Young's modulus, the BM phantom's thermal response to PPG concentration is measured and evaluated. 1.5% and 1.7% gellan gum phantoms are also tested with varying PPG to observe how thermal conductivity changes as gellan gum concentration is altered. The 12 samples (four for every gellan gum composition) undergo steady-state heating using the testing apparatus illustrated in Fig. 1(b).

Fig. 3(a) shows the temperature vs time response for 40 % PPG. The calculated values are shown in Table II. Fig.

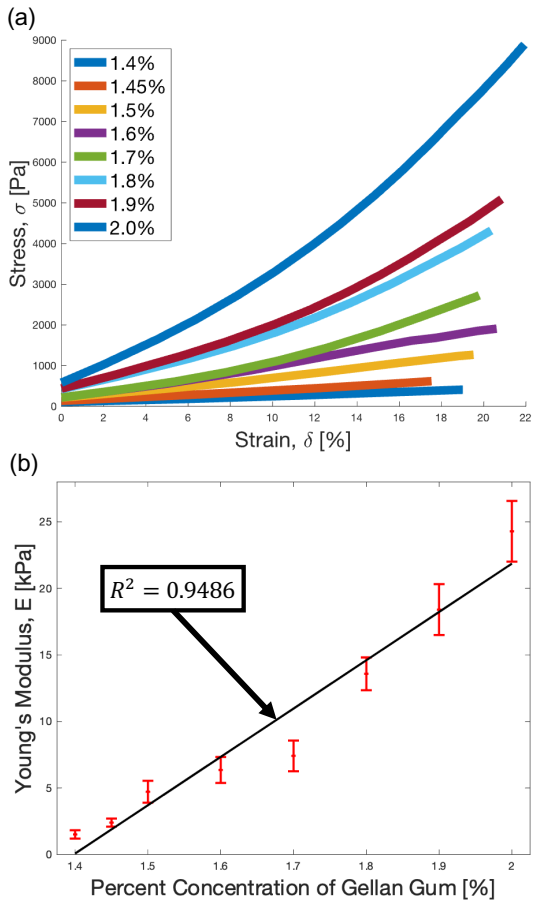

Fig. 2. (a) Stress v.s. strain curves for each tested gellan gum composition, ranging from 1.4% to 2.0% concentrations. (b) Average E and standard deviations for each gellan gum composition with linear regression ($R^2 = 0.9486$).

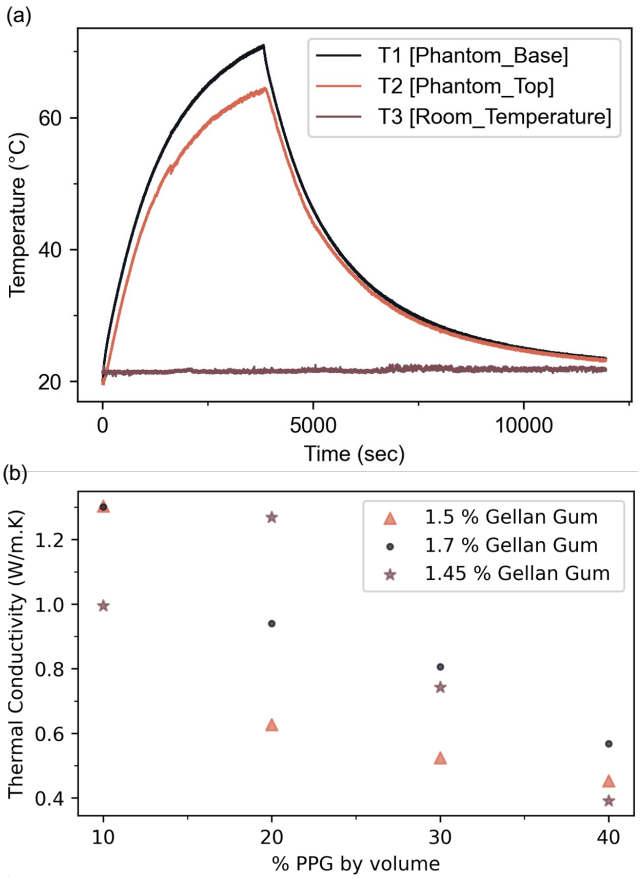

Fig. 3. (a) Temperature response of BM phantom (1.7% gellan gum and 40% PPG) at constant heat flux and subsequent cooling over time. (b) The relationship between κ v.s. PPG Volume% for BM phantom.

3(b) depicts the relationship between κ and % PPG. 20% PPG at 1.45 % gellan gum is an outlier and does not fit the trend. Unexpected outcomes observed are attributed to thermocouple probe displacement from the initial position, resulting in a deviation from the intended methodology and the occurrence of errors.

TABLE II

PPG CONCENTRATION AND CORRESPONDING THERMAL CONDUCTIVITY FOR GELLAN GUM

PPG % Volume	κ [W(mK)$^{-1}$] (1.45% gellan gum)	κ [W(mK)$^{-1}$] (1.5% gellan gum)	κ [W(mK)$^{-1}$] (1.7% gellan gum)
10	0.995	1.3036	1.3011
20	1.269	0.6273	0.9397
30	0.743	0.5240	0.8056
40	0.391	0.4529	0.5677

C. Photoablation Response and OCT Visualisation

BM phantoms composed of pure gellan gum are optically transparent to the OCT laser light. The addition of Intralipid emulsion increases the scattering coefficients of the material. Samples of the 1.45 % gellan gum phantom (E = 1.507 $\pm$ 0.313 kPa) with varying Intralipid volumes (0.25, 0.5, 0.75, 1.0 mL) are prepared and ablated at a fixed duty cycle (4 W laser power) and irradiance time (1 sec). The laser parameters are selected to generate a crater with a depth greater than 72 μm based on empirical results. Fig. 4 and Table III show the generated B-scans of the 1.45% BM phantoms both with and without Intralipid.

IV. DISCUSSION

The developed BM phantom properties are tuned to match reported values of brain tissue (gray matter) based on experiments. The mechanical properties of the phantoms are validated by conducting indentation tests to measure Young's modulus, reaching a desired gellan gum concentration of 1.4 to 1.45% for mimicking grey matter. In addition, gellan gum phantoms with concentrations above and within 2% can be used to produce BM phantoms to mimic the mechanical properties of brain tumors [16]. Phantoms containing PPG result in a faster curing time compared to phantoms comprising only gellan gum. The stiffness of the phantoms also increases due to the addition of PPG. Incorporating Intralipid emulsion into the gellan gum phantoms also increases the stiffness of the sample.

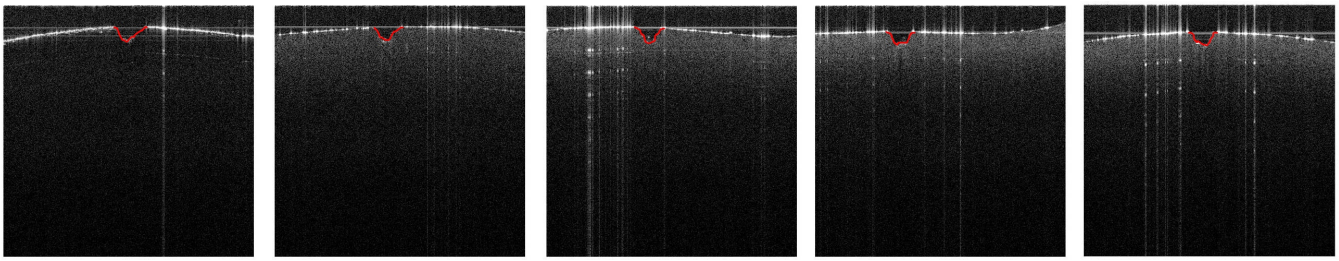

Fig. 4. B-scan of ablation crater (in red) under the OCT for a BM phantom with 1.50% gellan gum and: (a) 0 mL Intralipid (b) 0.25 mL Intralipid (c) 0.50 mL Intralipid (d) 0.75 mL Intralipid (e) 1 mL Intralipid.

Although the two components used (gellan gum and PPG) for the BM phantom are similar to [22], the values for Young's modulus and thermal conductivity differ significantly. The proposed work utilizes a different method to calculate E compared to Chen et al. [22]. The measured E values are to be compared to the E values of brain tissue in [15]. Thus, the proposed work calculates E using the method described in Budday et al. [15] for a fair comparison. Possible reasons for the difference in thermal conductivity can be attributed to the use of the longitudinal heat transfer method, which can produce inherent error in the values due to the assumption of one-dimensional heat flow, imperfect insulation, difference in distances between thermocouples at higher temperatures, and contact between phantom, heat source, and heat sink. Methods utilizing a single thermistor can be explored to calculate κ and observe the progression at different temperatures rather than only steady-state conditions. This will also reduce the experiment duration and allow for repeatability tests which are lacking in the presented work.

The κ for BM phantoms consistently decrease with the addition of PPG and is close to the values in the literature. Based on the literature, it is to note that the location and method of reporting of thermal conductivity of brain tissues is an important consideration, as the κ for *in vivo* v.s. *in vitro* measurement of tissue properties can vary [32]. Similar observations are reported regarding elastic properties of rabbit brain with approximately 47% higher shear modulus value *in vivo*, compared to *ex vivo* [33]. Although the study in [33] focuses on shear modulus, the difference in *in vivo* and *ex vivo* environments can result in different Young's modulus values as well.

As seen in Fig. 4, the addition of Intralipid increases the scattering coefficient of BM phantoms with 0.50% Intralipid and above, showing clear ablated crater shapes under the OCT. Increasing Intralipid concentration provides a more dense and higher resolution shape to the crater. A delineating boundary line between air and phantom is also visible in all five cases. No substantial change in crater depth and width is observed due to the addition of Intralipid, as shown in Table III.

TABLE III
INTRALIPID EMULSION CONCENTRATION AND CORRESPONDING YOUNG'S MODULUS OF BM PHANTOM WITH GELLAN GUM 1.50% MASS FRACTION

Intralipid % mass	Observation
0 mL	Air tissue interface distinct
0.25 mL	Ablation crater can be visualized
0.50 mL	Ablation crater can be visualized. Speckle noise present
0.75 mL	Denser phantom visualization below the surface. Speckle noise present
1.00 mL	Denser phantom visualization below the surface. Speckle noise present

A. Limitation

The results presented show that gellan gum phantoms can be tuned both mechanically and thermally independently, but the thermal parameters affect the mechanical properties. Additional work must be done to implement both properties simultaneously to produce a realistic brain phantom for photoablation studies.

The BM phantoms developed in this study have a shorter shelf life than desired, as it dehydrates and becomes stiffer over time. A method to preserve such phantoms over a longer period of time is essential for longitudinal medical robotics experiments. The current phantom design comprises a single layer and does not represent the multi-layer structure of a real brain. Addressing multi-layer tissue design utilizing CT-derived positive molds will also allow embedding tumor phantoms inside BM phantoms for photoablation and OCT visualization.

B. Future Work

The relationship between Intralipid, PPG, and gellan gum needs to be further explored to generate a singular phantom that mimics the mechanical, thermal, and optical properties similar to that of real brain tissue. Additional experiments in determining κ can address the uncorrelated results shown in Fig. 3(b), as only one experiment per PPG concentration is conducted. To add, solutions that reduce the thermal conductivity of the phantom without increasing the stiffness can be explored and tested.

The proposed work also conducts optical property experiments qualitatively. Future work will explore a quantitative analysis of the scattering coefficient of BM phantoms. To add, BM phantom response characterization to ablation will be explored with a singular phantom component that follows the geometrical constraints of the brain.

V. Conclusion

The proposed work presents a functionally tunable brain-mimicking (BM) phantom with the ability to emulate the mechanical, thermal, and optical properties of brain tissue for photoablation studies and OCT-based visualization. This work builds upon previous years of TM phantom research to present model designs addressing the specific constraints of laser-tissue interaction, such as high water content and mechanical and thermal properties similar to brain tissue. By tuning the gellan gum concentration of BM phantoms, Young's modulus as low as 2 kPa and thermal conductivity values of 0.5240 $W(mK)^{-1}$ similar to gray matter (0.53 to 0.56 $W(mK)^{-1}$) are achieved. The results of the experiments also show that scattering agents added to the BM phantom can tune the visibility of the phantom under the OCT laser. The resulting BM phantom responds to photoablation, and the resulting crater can be clearly visualized using OCT. For applications involving OCT or other laser-based imaging methods, it is recommended to add a minimum of 0.5 mL of Intralipid for clear visualization. Creating such phantoms that serve as surrogates for real brain tissue is an integral component of preparing realistic and repeatable experimental platforms to test future research advancements in robotic and laser-based high-precision surgery.

VI. Acknowledgment

Research reported in this publication was supported by the National Institutes of Health under award number R01EB030982. The content is solely the responsibility of the authors and does not necessarily represent the official views of the National Institutes of Health. The authors would like to thank the members of the Brain Tool Lab and Duke Robotics for their valuable feedback and critique.

References

[1] A. E. Forte, S. Galvan, F. Manieri, F. R. y Baena, and D. Dini, "A composite hydrogel for brain tissue phantoms," *Materials & Design*, vol. 112, pp. 227–238, 2016.

[2] M. Navarro-Lozoya, M. S. Kennedy, D. Dean, and J. I. Rodriguez-Devora, "Development of phantom material that resembles compression properties of human brain tissue for training models," *Materialia*, vol. 8, p. 100438, 2019.

[3] S. R. Oca, H. J. Strong, Amy, D. M. Buckland, and L. J. Bridgeman, "Development and testing of a durable and novel breast phantom for robotic autonomous ultrasound systems," *Journal of Medical Robotics Research*, 2022.

[4] Z.-J. Chen, G. T. Gillies, W. C. Broaddus, S. S. Prabhu, H. Fillmore, R. M. Mitchell, F. D. Corwin, and P. P. Fatouros, "A realistic brain tissue phantom for intraparenchymal infusion studies," *Journal of neurosurgery*, vol. 101, no. 2, pp. 314–322, 2004.

[5] A. D. Maxwell, T.-Y. Wang, L. Yuan, A. P. Duryea, Z. Xu, and C. A. Cain, "A tissue phantom for visualization and measurement of ultrasound-induced cavitation damage," *Ultrasound in medicine & biology*, vol. 36, no. 12, pp. 2132–2143, 2010.

[6] M. Ilami, R. J. Ahmed, A. Petras, B. Beigzadeh, and H. Marvi, "Magnetic needle steering in soft phantom tissue," *Scientific reports*, vol. 10, no. 1, pp. 1–11, 2020.

[7] M. Tucker, G. Ma, W. Ross, D. M. Buckland, and P. J. Codd, "Creation of an automated fluorescence guided tumor ablation system," *IEEE Journal of Translational Engineering in Health and Medicine*, vol. 9, pp. 1–9, 2021.

[8] R. Li, C. Jackovatz, S. Xu, B. J. Wood, H. Ren, K. R. Nilsson, and T. Zion, "A ct-visible thermal ablation phantom," in *2020 International Symposium on Medical Robotics (ISMR)*. IEEE, 2020, pp. 30–35.

[9] D. L. Collins, A. P. Zijdenbos, V. Kollokian, J. G. Sled, N. J. Kabani, C. J. Holmes, and A. C. Evans, "Design and construction of a realistic digital brain phantom," *IEEE transactions on medical imaging*, vol. 17, no. 3, pp. 463–468, 1998.

[10] B. Aubert-Broche, A. C. Evans, and L. Collins, "A new improved version of the realistic digital brain phantom," *NeuroImage*, vol. 32, no. 1, pp. 138–145, 2006.

[11] A. Mohammadi, L. Bianchi, S. Korganbayev, M. De Landro, and P. Saccomandi, "Thermomechanical modeling of laser ablation therapy of tumors: Sensitivity analysis and optimization of influential variables," *IEEE Transactions on Biomedical Engineering*, vol. 69, no. 1, pp. 302–313, 2021.

[12] T. Asshauer, G. Delacretaz, E. Jansen, A. Welch, and M. Frenz, "Pulsed holmium laser ablation of tissue phantoms: correlation between bubble formation and acoustic transients," *Applied Physics B*, vol. 65, no. 4, pp. 647–657, 1997.

[13] B. Majaron, P. Plestenjak, and M. Lukač, "Thermo-mechanical laser ablation of soft biological tissue: modeling the micro-explosions," *Applied Physics B*, vol. 69, no. 1, pp. 71–80, 1999.

[14] A. Kabiri and M. R. Talaee, "Thermal field and tissue damage analysis of moving laser in cancer thermal therapy," *Lasers in Medical Science*, vol. 36, no. 3, pp. 583–597, 2021.

[15] S. Budday, R. Nay, R. de Rooij, P. Steinmann, T. Wyrobek, T. C. Ovaert, and E. Kuhl, "Mechanical properties of gray and white matter brain tissue by indentation," *Journal of the mechanical behavior of biomedical materials*, vol. 46, pp. 318–330, 2015.

[16] D. C. Stewart, A. Rubiano, K. Dyson, and C. S. Simmons, "Mechanical characterization of human brain tumors from patients and comparison to potential surgical phantoms," *PloS one*, vol. 12, no. 6, p. e0177561, 2017.

[17] P. Hasgall, F. Di Gennaro, C. Baumgartner, E. Neufeld, B. Lloyd, M. Gosselin, D. Payne, A. Klingenböck, and N. Kuster, "It'is database for thermal and electromagnetic parameters of biological tissues, version 4.0," *IT'IS*, 2018.

[18] R. L. Mcintosh and V. Anderson, "A comprehensive tissue properties database provided for the thermal assessment of a human at rest," *Biophysical Reviews and Letters*, vol. 5, no. 03, pp. 129–151, 2010.

[19] A. Mohammadi, L. Bianchi, S. Asadi, and P. Saccomandi, "Measurement of ex vivo liver, brain and pancreas thermal properties as function of temperature," *Sensors*, vol. 21, no. 12, p. 4236, 2021.

[20] A. I. Farrer, H. Odéen, J. de Bever, B. Coats, D. L. Parker, A. Payne, and D. A. Christensen, "Characterization and evaluation of tissue-mimicking gelatin phantoms for use with mrgfus," *Journal of therapeutic ultrasound*, vol. 3, no. 1, pp. 1–11, 2015.

[21] A. V. Bykov, A. P. Popov, M. Kinnunen, T. Prykäri, A. V. Priezzhev, and R. Myllylä, "Skin phantoms with realistic vessel structure for oct measurements," in *Laser Applications in Life Sciences*, vol. 7376. SPIE, 2010, pp. 118–124.

[22] R. K. Chen and A. Shih, "Multi-modality gellan gum-based tissue-mimicking phantom with targeted mechanical, electrical, and thermal properties," *Physics in Medicine & Biology*, vol. 58, no. 16, p. 5511, 2013.

[23] R. Valli and R. Clark, "Food stabilisers, thickeners and gelling agents ed a imeson," 2010.

[24] F. Duck, "Physical properties of tissue: a comprehensive reference book (london; san diego: Academic)," 1990.

[25] O. A. Smidsrod, A. Haug, B. Lian, A. Huhtikangas, W. B. Pearson, and V. Meisalo, "Properties of poly(1,4-hexuronates) in the gel state. i. evaluation of a method for the determination of stiffness." *Acta Chemica Scandinavica*, vol. 26, pp. 71–78, 1972.

[26] J. Bradbeer, R. Hancocks, F. Spyropoulos, and I. Norton, "Self-structuring foods based on acid-sensitive low and high acyl mixed gellan systems to impact on satiety," *Food hydrocolloids*, vol. 35, pp. 522–530, 03 2014.

[27] M. Moresi and M. Bruno, "Characterisation of alginate gels using quasi-static and dynamic methods," *Journal of Food Engineering*, vol. 82, no. 3, pp. 298–309, 2007. [Online]. Available: https://www.sciencedirect.com/science/article/pii/S0260877407001227

[28] L. Maggi, G. A. Cortela, M. A. von Kruger, C. A. Negreira, and W. C. A. Pereira, "Ultrasonic attenuation and speed in phantoms made of pvcp and evaluation of acoustic and thermal properties of ultrasonic phantoms made of polyvinyl chloride-plastisol (pvcp)," in *IWBBIO*, 2013.

[29] W. A. Ross, W. M. Hill, K. B. Hoang, A. S. Laarakker, B. P. Mann, and P. J. Codd, "Automating neurosurgical tumor resection surgery: Volumetric laser ablation of cadaveric porcine brain with integrated surface mapping," *Lasers in surgery and medicine*, vol. 50, no. 10, pp. 1017–1024, 2018.

[30] G. Ma, W. A. Ross, I. Hill, N. Narasimhan, and P. J. Codd, "A novel laser scalpel system for computer-assisted laser surgery," in *2019 International Conference on Robotics and Automation (ICRA)*. IEEE, 2019, pp. 386–392.

[31] K. Manickam, R. R. Machireddy, and S. Seshadri, "Characterization of biomechanical properties of agar based tissue mimicking phantoms for ultrasound stiffness imaging techniques," *Journal of the Mechanical Behavior of Biomedical Materials*, vol. 35, pp. 132–143, 2014. [Online]. Available: https://www.sciencedirect.com/science/article/pii/S1751616114000897

[32] Z. Liu, Z. Liao, D. Wang, C. Wang, C. Song, H. Li, and Y. Liu, "Recent advances in soft biological tissue manipulating technologies," *Chinese Journal of Mechanical Engineering*, vol. 35, no. 1, pp. 1–34, 2022.

[33] Y.-L. Liu, D. Liu, L. Xu, C. Su, G.-Y. Li, L.-X. Qian, and Y. Cao, "In vivo and ex vivo elastic properties of brain tissues measured with ultrasound elastography," *Journal of the mechanical behavior of biomedical materials*, vol. 83, pp. 120–125, 2018.